ACES Asian Chemical Editorial Society

DOI: 10.1002/cnma.201900126

CHEMNANOMAT
Full Paper

# Insight into Catalytic Mechanisms for the Reduction of Nitrophenol via Heterojunctions of Gold Nanoclusters on 2D Boron Nitride Nanosheets

Bingping Liu,[a] Shihai Yan,[a] Aitang Zhang,[b] Zhongqian Song,[c] Qinxing Sun,[a] Bingbing Huo,[b] Wenrong Yang,[d] Colin J. Barrow,[d] and Jingquan Liu*[b]

**Abstract:** Gold nanoclusters were synthesized and homogeneously distributed on boron nitride nanosheets (BNNSs) to form AuNC@BNNSs nanohybrids. Compared to pure gold nanoclusters, the nanohybrid not only exhibits much better catalytic activity for the reduction of 4-nitrophenol (4-NP), but also prevents gold nanoclusters from aggregation. We found that the catalytic performance of AuNC@BNNSs nanohybrid increased with decreasing pH and increasing temperature of the reaction environment. The catalytic mechanism of the nanohybrid was thoroughly explored by density functional theory (DFT). It was concluded that the catalytic activity should be caused by repeated electron transfer on HOMO between 4-NP and BNNSs, which was mediated by the surface-bound gold nanoclusters. Furthermore, it was observed that the actual reducing agent is molecular hydrogen rather than borohydride. The present methodology could be generalized to the synthesis of other metallic nanoparticle@BNNSs nanohybrids as promising heterogeneous catalysts for varied catalytic reactions.

## Introduction

For decades, gold-related catalysts have been applied in many catalytic reactions such as hydrogenation of aldehydes, oxidation of alcohols and reduction of 4-nitrophenol, owing to their stable chemical properties, facile synthesis, low toxicity and highly effective catalytic performance under mild conditions.[1] It is commonly accepted that the high activity of the catalyst is attributed to their high surface-to-volume ratio, surface geometric effect, the electronic properties, and the quantum size effect, which are determined by the size of particles. Jin et al. use the free electron theory to estimate what size of gold nanoparticles will exhibit distinct quantum size effects.[2] It was demonstrated that the size of ~2 nm is that at which electronic energy quantization will become important, and below this size the collective plasmon mode will no longer be supported. Some catalytic activities of gold particles, such as hydrogenation of aldehydes, oxidation of alcohols and reduction of 4-nitrophenol, appear when their size is reduced down to 1–5 nm, while the activity decreases dramatically as the size of gold particles is enlarged and the bulk noble metals are almost catalytically inert.[3] However, during the catalytic reaction, the small sized catalysts are vulnerable to self-aggregation into larger particles due to their high surface area and surface energy, which could easily result in deactivation or loss of their catalytic activities.[4] As far as we know, nanostructured catalyst supports can efficiently overcome this inherent shortcomings. For example, gold and other noble metal nanoparticles have been loaded onto ultrathin 2-dimensional (2D) nanosheets to afford 0D/2D nanocomposites,[5] which displayed superior performance compared with their corresponding nanoparticles used alone or supported on the insulating oxide, such as $ZrO_2$,[6] hydrotalcite,[3a] c-$Al_2O_3$, silica-alumina and various zeolites,[7] MgO[8] or $TiO_2$.[9] This enhanced performance results from the distinct properties of 2D materials such as the large surface area, high chemical stability, etc.[5b,10]

Graphene,[11] molybdenum disulfide ($MoS_2$),[12] carbon nitride ($C_3N_4$)[13] and boron nitride (BN) have been chosen as efficient supports to immobilize and stabilize noble metal particles as catalysts. Among the available supports, hexagonal boron nitride nanosheets (h-BNNSs) is a promising candidate for the fabrication of hybrids due to its atomic-thick sheet structure, high thermal conductivity, unique insulation and chemical and thermal inertness, especially when hazardous environments are involved. So far, h-BNNSs have been widely used as the support for some metal nanoparticles of Fe,[14] Pt,[15] Pd,[15c,16] Ag[17] and Au,[18] to enhance their catalytic performance. For example, Meyer et al.[16] and Sun et al.[15c] have decorated BNNSs with Pd nanoparticles for catalytic hydrogenation of lactose and nitro aromatics. The resultant Pd – BNNSs catalyst exhibited high catalytic activity and recyclability, demonstrating that BNNSs can serve as a promising platform for fabrication of heteroge-

[a] Dr. B. Liu, Dr. S. Yan, Dr. Q. Sun
Collegeof Chemistry and Pharmaceutical Sciences
Changcheng Road 700, Qingdao Agricultural University,266109, China
[b] Dr. A. Zhang, B. Huo, Prof. Dr. J. Liu
College of Materials Science and Engineering
Institute for Graphene Applied Technology Innovation
Ningxia Road 308, Qingdao University, 266071, China
E-mail: jliu@qdu.edu.cn
[c] Dr. Z. Song
Engineering Laboratory for Modern Analytical Techniques
Changchun Institute of Applied Chemistry, Chinese Academy of Sciences, Changchun 130022, China
[d] Prof. Dr. W. Yang, Prof. Dr. C. J. Barrow
Centre for Chemistry and Biotechnology
School of Life and Environmental Sciences
Deakin University, Geelong Waurn Ponds Campus, VIC 3216, Australia

Supporting information for this article is available on the WWW under https://doi.org/10.1002/cnma.201900126

neous catalysts. Xu et al. reported a facile strategy to synthesize Ag nanoparticles on the surface of BNNSs modified with a thin layer of tannic acid-ferric ion (TA-Fe) complex.[17a] The as-synthesized BNNSs/Ag nanohybrids exhibited excellent catalytic activity in reduction of 4-nitrophenol. Recently, BNNSs were decorated with Au nanoparticles due to their unique properties, as described above. Fu et al. synthesized BNNSs-AuNP composite from hydroxyl-BNNSs without adding reducing agent, which exhibited excellent catalytic and electrocatalytic activity in the degradation of Rhodamine B (Rh B) and electro-oxidation of hydrazine.[19] The enhanced catalytic activity should be attributed to dispersion stability of the noble metal nanoparticles on the support. Although exciting progress has been made, it is still a grand challenge to achieve a fundamental understanding of heterogeneous catalytic performance for nanostructured materials of noble metal- BNNSs with programmable structures and predictable properties.

In this work, the nanohybrids (AuNC@BNNSs) of gold nanoclusters (AuNCs) and 2D BNNSs were synthesized and their catalytic activity were investigated via reduction of nitrophenol, which was one of the poisonous pollutants in waste water. The AuNCs were synthesized with an average size of 1.5 nm on ultrathin BNNSs, and exhibited much higher catalytic activity than pure AuNCs. Here we also present a detailed mechanistic study on the reduction of 4-nitrophenol (4-NP) in the presence of AuNC@BNNSs nanohybrid using density functional theory (DFT). We found that the enhanced catalytic performance is mainly caused by repeated electron transfer between 4-NP and AuNCs during the reaction. More interestingly, we have for the first time demonstrated that the actual reducing agent for the reduction of 4-NP to 4-AP is molecular hydrogen rather than borohydride. Moreover, this reduction strategy does not require rigorous conditions or toxic agents, and therefore could be developed into an efficient and green approach for the fabrication of noble-metal loading catalysts with significantly enhanced catalytic activity.

## Results and Discussion

### Characterizations of Stepwise Preparation of AuNC@ BNNSs Nanohybrid

The preparation of AuNC@BNNSs nanohybrid is illustrated in Scheme 1. Initially, the bulky hexagonal BN (h-BN) was first exfoliated by mechanical ball milling in the presence of a mixed aqueous solution of NaOH and KOH. During the ball milling process, bulk BN powder was edge-opened via the strong shearing force and collision mediated by ball milling, followed by intercalation of the ions, including $Na^+$, $K^+$ and $OH^-$ ions, into h-BN layers to assist further exfoliation. The exfoliated BNNSs were characterized by transmission electron microscopy (TEM) and Fourier transform infrared (FTIR) spectrometry (Figure S1 and Figure S2). After exfoliation, AuNC@BNNSs nanohybrid was synthesized via a thermal co-reduction of $HAuCl_4$ and BNNSs suspension at 90 °C in the presence of GSH, a mild reducing agent that reduced $Au^{3+}$ into Au. The nucleation of

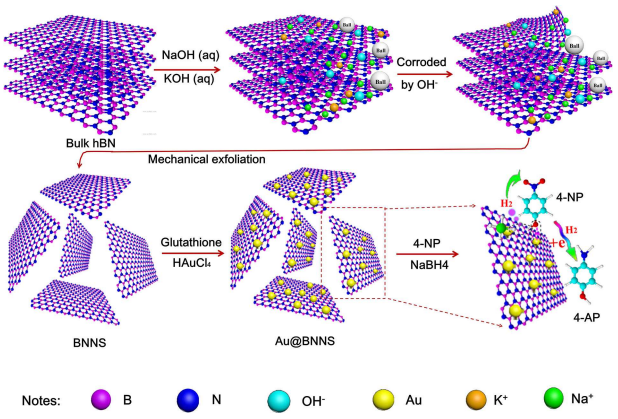


**Scheme 1.** Schematic illustration for the exfoliation of h-BN and the preparation of AuNC@BNNSs nanohybrid as catalyst for the reduction of 4-nitrophenol (4-NP).

Au atoms led to the formation of AuNCs and homogeneously distribution on 2D BNNSs.[20] In addition, the hydroxylated BNNSs can also assist the reduction of $Au^{3+}$ into $Au^0$ as evidenced by Fu el at.[19] In this work, the reaction time was optimized and the experiments were carried out for 12 h, 15 h, 18 h, 21 h and 24 h, respectively. (Figure S3) It was observed that the size of AuNCs was slightly increased when the reaction time increased from 12 h to 15 h, and the size was almost kept constant even the reaction time was further enlarged. Therefore, the optimal time was set to be 12 h. We first characterized the morphology of AuNC@BNNSs nanohybrid using TEM and observed that AuNCs were uniformly distributed on the surface of BNNSs without aggregation (Figure 1a). The inset indicates the narrow size distribution of AuNCs and an average size of 1.5 nm was derived. High resolution transmission electron microscopy (HRTEM) images of the AuNCs revealed that both single crystalline lattice and twinned polyhedral states existed, as shown in Figure 1b and its inset. The HRTEM image (Figure 1b) shows some ordered lattice fringes with average spacing of 0.236 nm and 0.204 nm, which corresponds to the (111) and (200) lattice spacing of AuNCs.[21] HRTEM image shows clear lattice fringes of the exfoliated h-BNNSs from the bulk BN precursor. As shown in Figure 1c, the number of layers of BNNSs is about 5 to 7. To analyze the chemical composition of the as-prepared AuNC@BNNSs nanohybrid, energy dispersive X-ray (EDX) spectrum and element mapping images were collected. The EDX profile, as shown in Figure 1d, clearly shows the presence of N and Au elements, whose contents (wt%) were calculated to be 25.7 and 10.54, respectively, according to their signal intensities. Consistent results were also obtained by element mapping images, as shown in Figure 1e. The crystal structure of the AuNCs was also investigated by selected area electron diffraction (SAED). As shown in Figure 1f, four d-spacing were found to be 2.4, 2.1, 1.4 and 1.3 Å, which correspond to the Au (111), Au (200), Au (220) and Au (331) Miller indices of fcc (face-centered cubic) gold crystals, respectively.[22] The chemical composition and structure of the AuNC@BNNSs nanohybrid were further confirmed by X-ray

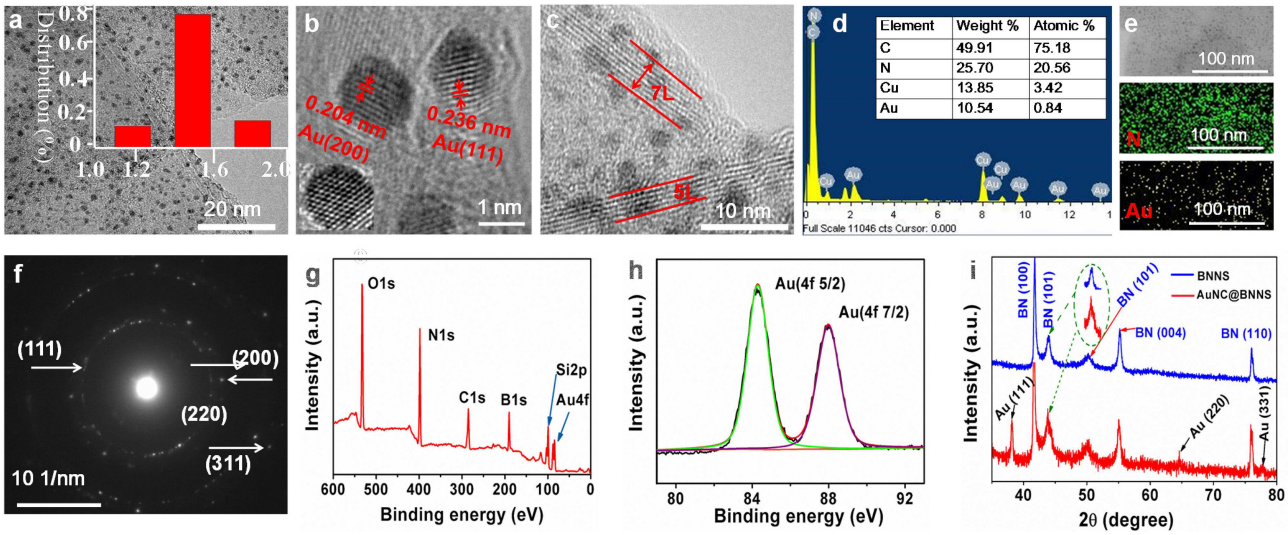


**Figure 1.** Typical TEM images of AuNC@BNNSs nanohybrid with different magnifications, XPS and XRD spectra. (a) Low-magnification TEM image of AuNC@BNNSs. The inset shows the size distribution of AuNCs. (b) High-magnification TEM image showing the single crystalline structure and multi-crystalline structure of AuNCs. (c) HRTEM image of BNNSs with clear latticefringes. (d) EDX spectrum of AuNC@BNNSs nanohybrid and the relative abundance of each element. (e) The elemental mappings of N and Au. (f) SAED pattern of AuNC@BNNSs. (g) Survey XPS spectrum of AuNC@BNNSs. (h) Au 4f narrow XPS scan spectra. (i) XRD patterns of BNNSs and AuNC@BNNSs.

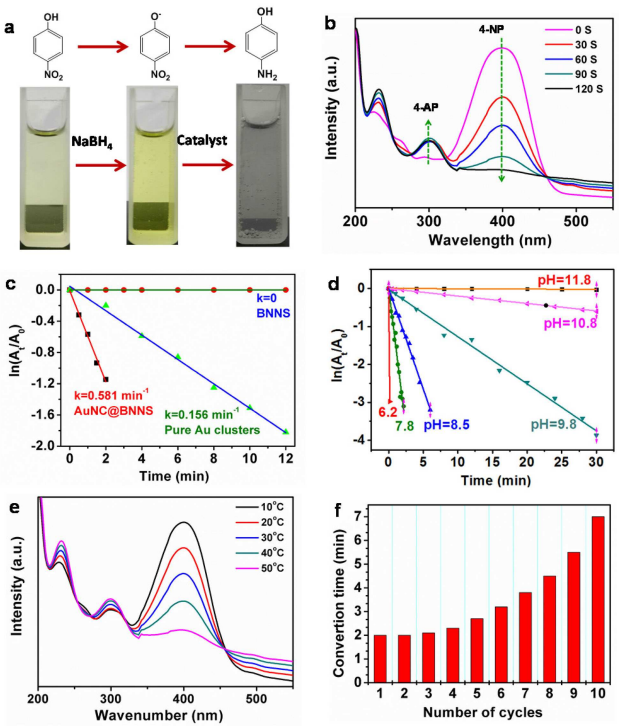


**Figure 2.** The catalytic performance of AuNC@BNNSs nanohybrid for reduction of 4-NP to 4-AP. (a) Reaction scheme representing reduction catalyzed by AuNC@BNNSs. (b) Time-dependent UV-vis absorption spectra at room temperature. (c) The plot of $\ln(A_t/A_0)$ versus time in the presence of BNNSs, AuNCs and AuNC@BNNSs as catalysts, respectively. (d) Determination of the rate constants for reduction at different pH values at room temperature. (e) UV-absorption spectra measured after 30 seconds at different temperatures. (f) The recyclability of AuNC@BNNSs as a catalyst for the reduction of 4-NP.

photoelectron spectroscopy (XPS) and X-ray diffraction (XRD) analyses. The survey spectrum of AuNC@BNNSs is illustrated in Figure 1g, where six peaks at 532.57 eV, 397.9 eV, 284.89 eV, 190.12 eV, 99.24 eV and 84.27 eV were observed, indicating the presence of O, N, C, B, Si and Au elements, respectively.

The peak of O1s and C1s are probably caused by contamination from the air, which is a common problem in XPS characterization.[23] The presence of Si is due to the utilization of silicon wafer. As shown in Figure 1h, the peak with binding energy of 84.27 eV corresponding to elemental Au, can be split into two peaks at 84.1 eV (Au 4f 7/2) and 87.9 eV (Au 4f 5/2), evidencing the presence of metallic Au in AuNC@BNNSs. The presence of metal Au is also confirmed by comparison of the XRD patterns between BNNSs and AuNC@BNNSs, which are shown in Figure 1i. The distinct characteristic peaks at 41.7°, 44.0°, 50.3°, 55.1° and 76.0° can be assigned to the (100), (101), (102), (004) and (110) crystallographic planes of h-BN (JCPDS no. 85-1068).[24] The additional peaks at 38.2°, 64.6° and 77.6° in the XRD pattern of the AuNC@BNNSs nanohybrid are attributed to the (111), (220) and (331) crystal faces of face-centered cubic (fcc) Au (JCPDS 65–2870).[25] It was also observed from Figure 1i that the peak at around 44.0° was overlapped by other two peaks at 43.9° and 44.3°, which should result from the crystal faces of BN (101) and Au (200).

### Catalytic Activity of AuNC@BNNSs for Reduction of 4-Nitrophenol Evaluation of Catalytic Performance

The catalytic performance of the as-prepared AuNC@BNNSs nanohybrid was evaluated via the well-known reduction reaction of 4-nitrophenol (4-NP) to 4-aminophenol (4-AP) in the presence of $NaBH_4$ at room temperature. As shown in Figure 2a,

the color of 4-NP solution immediately changed from light yellow to yellowish green when $NaBH_4$ was added due to deprotonation of 4-NP. Also, the absorption band (λmax) was shifted from 340 to 400 nm due to the formation of the 4-nitrophenolate ion. After addition of AuNC@BNNSs, the catalytical kinetics of the reduction was monitored in situ by successive measurement of UV-vis absorption of the reaction mixture every 30 seconds at room temperature and the results are illustrated in Figure 2b. It was observed that the peak at 400 nm for the absorption of 4-nitrophenolate ions decreased gradually with the increasing reaction time. The characteristic peak of 4-AP appeared at 300 nm during the reduction process and the reaction is completely finished within 2 min. Meanwhile, the color of the reaction mixture changed from yellowish green to colorless upon the addition of the AuNC@BNNSs catalyst. Since the concentration of $NaBH_4$ largely exceeded that of 4-NP in this experiment, the reduction can be evaluated by a pseudo-first-order kinetic behavior with respect to 4-NP, which can be described by the equation as follows:

$$\ln\left(A_t/A_0\right) = -kt$$

Where, $A_0$ and $A_t$ are the absorbance values of 4-NP at time of 0 and t, respectively, and k is the apparent rate constant. The plot of ln ($A_t/A_0$) against reaction time is shown in Figure 2c, from which the rate constant, k, was calculated to be 0.581 $min^{-1}$ in the presence of AuNC@BNNSs as catalyst. To further evaluate the synergistic effect of AuNC@BNNSs nanohybrid on their excellent catalytic performance, the comparison experiments were carried out with BNNSs and pure AuNCs as catalysts, the rate constants were measured to be 0 and 0.156 $min^{-1}$, respectively. The catalyst turnover number (TON) and the turnover frequency (TOF) are two important parameters used for comparing catalyst efficiency. In heterogeneous catalysis, the TON is the number of reactant molecules that 1 g of catalyst can convert into products.[26] The TOF can be simply obtained by TON/time. The TOF of AuNC@BNNSswas calculated to be $14.7\times10^{16}$ molecules/g/s. Therefore, it can be concluded that AuNCs is the effective catalyst and the presence of BNNSs can significantly improve the catalytic activity. Compared with other similar catalysts, the AuNC@BNNSs shows better catalytic activity (Table 1).

Since the catalytic activity of the catalyst is generally affected by temperature and pH, we then carried out control experiments at different pH values and different temperatures, and the results are shown in Figure 2d and Figure 2e. To investigate the effect of pH, the UV-vis absorbance spectra are measured at different pH values of 6.2, 7.8, 8.5, 9.8, 10.8 and 11.8 (Figure S4) and the plots of ln ($A_t/A_0$) versus the reaction time at different pH values were derived as shown in Figure 2d. It is clear that the catalytic activity was significantly enhanced with decreasing of the pH. When the pH of reaction mixture was less than 6.2, the reaction was completed in less than 30 seconds. Conversely, no reaction occurs when the pH was above 11.8. Furthermore, we observed that the absorption intensity decreased with the increasing temperature (Figure 2e). When the temperature was 10 °C, the absorption intensity only decreased slightly. However, when the temperature reached 50 °C, the intensity was close to zero in 30 seconds. Therefore, the catalytic activity of AuNC@BNNSs increased with the decreasing pH and increasing temperature.

The recyclability, another critical factor to assess a catalyst, was measured by comparing the conversion time from 4-NP to 4-AP, in the presence of the catalysts recovered after different recycles. As shown in Figure 2f, the conversion time only slightly increased in the first three recycles. However, after 10 recycles the conversion time increased to 3.5 times longer. To explore the origin of the decrease of catalytic activity, the TEM images of the recovered catalyst were obtained after 5 recycles. As shown in Figure S5 there was almost no further morphology change observed for AuNC@BNNSs after 5 recycles, and the AuNCs were still homogeneously distributed on BNNSs. The average size of AuNCs only slightly decreased compared with those freshly prepared, which indicated the good stability of the clusters. Compared Figure S5a with Figure S5b, the distribution of AuNCs was sparser and the size was smaller after the five cycles, which should be caused by strong centrifugal force,resulting in the loss and disintegration of catalyst during centrifugation and the reduced catalytic activity.

**Table 1.** Comparison of $C_{NaBH4}$, $C_{4\text{-}NP}$ and the rate constant (k) for the reduction of 4-NP with different catalysts.

| Catalysts | $CNaBH_4$ (M) | $C_{4\text{-}NP}$ (mM) | k ($min^{-1}$) | Ref. |
|---|---|---|---|---|
| BNNS-Ag | 0.4 | 0.4 | 0.163 | 34 |
| Ag/BNNS | 0.2 | 0.1 | 0.428 | 36 |
| BNNS-AuNP | 0.05 | 0.1 | 0.05 | 38 |
| Free AuNCs | 0.02 | 0.2 | 0.156 | This work |
| AuNC@BNNS | 0.02 | 0.2 | 0.581 | This work |

## Mechanism for the Hydrogenation of 4-Nitrophenol

To investigate the origin of the excellent catalytic performance of AuNC@BNNSs nanohybrid, density functional theory (DFT) calculations were carried out using a suite of Gaussion 09 programs and the computational details were described in the supporting information. In the reduction of 4-NP, $NaBH_4$ was added as the reducing agent. However, the hydrolysis of $NaBH_4$ often occurs in aqueous medium to generate molecular hydrogen, especially in protic solutions, and molecular hydrogen is also an important reducing agent. Therefore, two possible reaction pathways for the reduction of 4-NP were assumed and calculated by DFT theory, where the reducing agent is either borohydride or molecular hydrogen. The reaction mechanism and the corresponding energy change for each step are demonstrated in Figure 3. As illustrated in Figure 3a, there are seven steps for the reaction between 4-NP and borohydride without catalyst. The reaction is initiated via dehydrogenation of borohydride to produce $H^+$ or $H^-$, which are both endothermic and uphill with energy changes of $+384\ Kcal\cdot mol^{-1}$ and $+236\ Kcal\cdot mol^{-1}$, respectively. Consequently, consecutive protonation reactions of 4-NP occur with

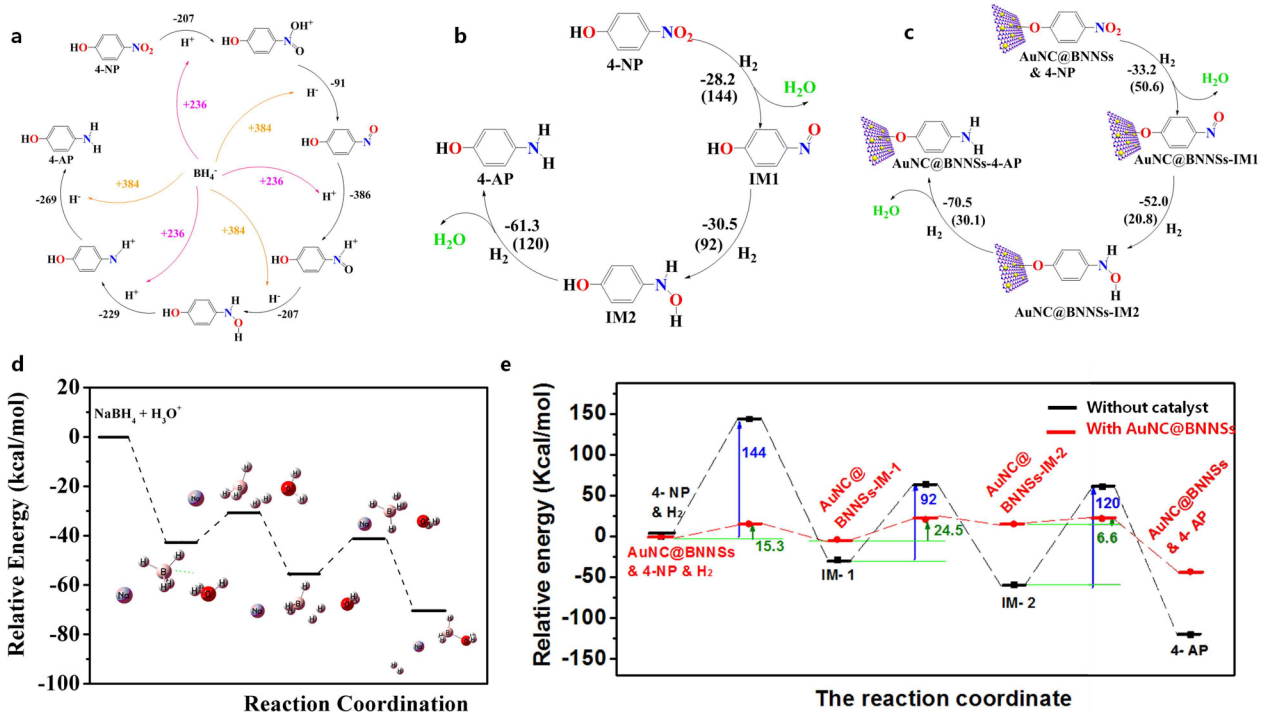


**Figure 3.** Scheme and energy profile showing the reduction reaction of 4-NP to 4-AP. (a) Reaction mechanism with borohydride as reducing agent in the absence of catalyst. (b) Scheme of the reaction mechanism for hydrolysis of borohydride. (c) and (d) The main reaction pathway in the absence and presence of AuNC@BNNSs as catalyst, respectively, when the reducing agent was molecular hydrogen. The values without bracket indicate the energy change and the ones in the bracket mean activation energies. (e) Energy profile of the reduction. Red lines show calculated values in the presence of AuNC@BNNSs as catalyst and black lines indicate the energy profile of the reduction in the absence of catalyst, when the reducing agent is molecular hydrogen. The blue values show the activation energies for different steps in the absence of catalyst and the green ones show activation energies with AuNC@BNNSs as catalyst.

$H^+$ or $H^-$ and all of these reactions are exothermic. If the reducing agent is molecular hydrogen, the reaction is initiated via the hydrolysis of borohydride, which is shown in Figure 3b. All the reactions are exothermic and the activation energy is not high enough so that the energy released in the first step can provide energy for all the following reactions. Therefore, hydrolysis of borohydride occurs at room temperature. Consequently, hydrogen molecule reacts with 4-NP step by step, which are summarized in Figure 3c and Figure 3d, and the corresponding energy change profile is illustrated in Figure 3e, Table S1 and Table S2. After molecular hydrogen is produced, molecular hydrogen is attracted by lone pair electrons on O atoms in the nitro group from 4-NP (Figure 3c and Figure 3d). Then, a water molecule is generated with the energy change of $-28.2$ Kcal·mol$^{-1}$ and $-3.9$ Kcal·mol$^{-1}$ in the absence or presence of the AuNC@BNNSs, with the activation energy of 144 Kcal·mol$^{-1}$ and 15.3 Kcal·mol$^{-1}$, respectively. Therefore, only one oxygen atom is left to bond with nitrogen, which is labeled to be intermediate 1 (IM1) and AuNC@BNNSs-IM1. Furthermore, the second molecular hydrogen is bonded to the lone pairs on N and O atoms to form the intermediates of IM-2 and AuNC@BNNSs-IM-2, downhill in the energy profile of $-30.5$ Kcal·mol$^{-1}$ and $+19$ Kcal·mol$^{-1}$, in which the activation energies decrease to 92 Kcal·mol$^{-1}$ and 24.5 Kcal·mol$^{-1}$, respectively. Finally, the lone pair electrons on both N and O atoms in the intermediates of IM-2 and AuNC@BNNSs-IM-2 attract another $H_2$ molecule to form 4-AP along with the energy change of $-61.3$ Kcal·mol$^{-1}$ and $-58.5$ Kcal·mol$^{-1}$ and the activation energies are 120 Kcal·mol$^{-1}$ and 6.6 Kcal·mol$^{-1}$, respectively. Throughout the mechanism, it can be concluded that the reactions require lower activation energies taken hydrogen molecule as a catalyst rather than borohydride, which proves the actual reducing agent is molecular hydrogen. As reported in previous studies,[27] the rate of hydrolysis of sodium borohydride in aqueous solution depends on pH and temperature. Lower pH and higher temperature promotes the production of hydrogen gas, which is consistent with the effect of pH value and temperature as discussed in this work.

To further qualitatively evaluate the catalytic performance of AuNC@BNNSs nanohybrid, Frontier molecular orbitals of the reactants, intermediates and products were calculated by the DFT method. As shown in Figure 4, the highest occupied molecular orbital (HOMO) of 4-NP are located predominantly on the benzene ring and O atom in the hydroxyl group and there are nearly no electrons on the nitro group. Therefore, it is difficult to release $H^+$ from hydroxyl groups to generate molecular hydrogen due to the high electron density. Meanwhile, the lower distribution of HOMO in nitro group (the second row in Figure 4) makes it difficult to attract molecular hydrogen. Therefore, the activation energy is relatively higher (144 Kcal·mol$^{-1}$). When the intermediate IM1 is formed, the HOMO locates primarily on remainder N=O group (the third

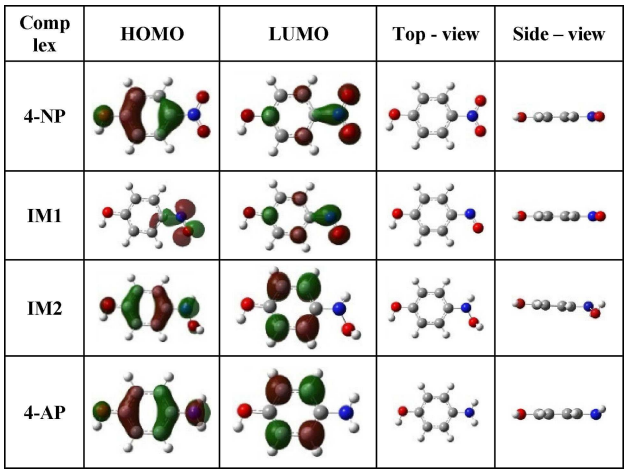


**Figure 4.** . Frontier molecular orbitals, side and top views of the optimized structure of reactants, intermediates and products in the absence of catalyst.

row in Figure 4), which favors to combine with molecular hydrogen. It is in accord with the notable decrease of activation energy (92 Kcal·mol$^{-1}$). The distribution of HOMO is homogeneous in both nitro group and benzene ring in IM2, so the reactivity of IM2 is higher than that of 4-NP, but lower than that of IM1.

As a control, frontier molecular orbitals, side and top views of the optimized structure of reactants, intermediates and products in the presence of AuNC@BNNSs are calculated. The results are illustrated in Figure S6 and the charges and distances of some atoms are summarized in Figure 5. As observed from HOMO of AuNC@BNNSs & 4-NP in row 2 of Figure S6, electrons in the HOMO transfer to AuNCs and nitro group in the presence of AuNC@BNNSs, which will benefit for the formation of molecular hydrogen and the formation of 4-nitrophenolate ions. Meanwhile, BNNSs made a contribution to keep nitrophenolate ions at the vicinity of AuNCs. As the molecular hydrogen gets closer to nitro group, the HOMO transfer completely from 4-NP to AuNCs and BNNSs (Seen AuNC@BNNSs & 4-NP & $H_2$ in Row 3 in Figure S6). The charges of some atoms and distances between atoms in AuNC@BNNSs & 4-NP & $H_2$ are illustrated in Figure 5a and 5b. The bond length of $H_5$–$H_6$, $O_2$–$N_4$, $O_3$–$N_4$ are 0.749 À, 1.347 À and 1.342 À, respectively. The charges for $O_2$, $O_3$ and $N_4$ atoms are−0.362,−0.341 and 0.296. The similar length of O–N and charges for $O_2$ and $O_3$ exhibit that there is a $\pi_3^4$ conjugated bond. As the reaction occurs, transition state of reactants is formed and shown as TS-AuNC@BNNSs & 4-NP & $H_2$ in Row 4 Figure S6. The charges and the distance between some atoms are illustrated in Figure 5c and 5d. The distance of $H_5$–$H_6$ enlarges to 1.056 À and $H_6$–$O_2$ decreases to 1.179 À, which means the bond in hydrogen bond is broken and $H_6$ favors to bond with $O_2$. Meanwhile, the bond length of $O_2$–$N_4$, $O_3$–$N_4$ changes into 1.403 À and 1.288 À, and the charges of $O_2$, $O_3$ and $N_4$ atoms are−0.439,−0.268 and 0.315, respectively. It is no doubt that$\pi_3^4$ conjugated bond in nitro group is broken.$O_2$–$N_4$ bond is gradually broken so that $O_2$ atom can form bond with H atoms to release water molecule and $O_3$-$N_4$ trend to form double bond. Finally, AuNC@BNNSs-IM1 is produce, in which HOMO and LOMO are displayed in Row 6 Figure S6. As a result, the formation of AuNC@BNNSs-IM1 is much easier than that of IM1 and the activation energy decreases from 144 Kcal·mol$^{-1}$ to 15.3 Kcal·mol$^{-1}$. As shown in Row 6 Figure S6, electrons on HOMO in the AuNC@BNNSs-IM1 are mainly distributed in N=O. The charges for N and O in N=O are shown in Figure 5e, which are 0.020 and−0.324, respectively. Therefore, the second molecule of hydrogen will be attracted by N and O and the transition state is illustrated in TS-AuNC@BNNSs-IM1 & $H_2$ in Row 7 in Figure S6. The distances between atoms are displayed in Figure 5g. When N–H and O–H bonds are formed, AuNC@BNNSs-IM2 is produced, shown in Row 8 Figure S6, in which the charges for N and O atoms

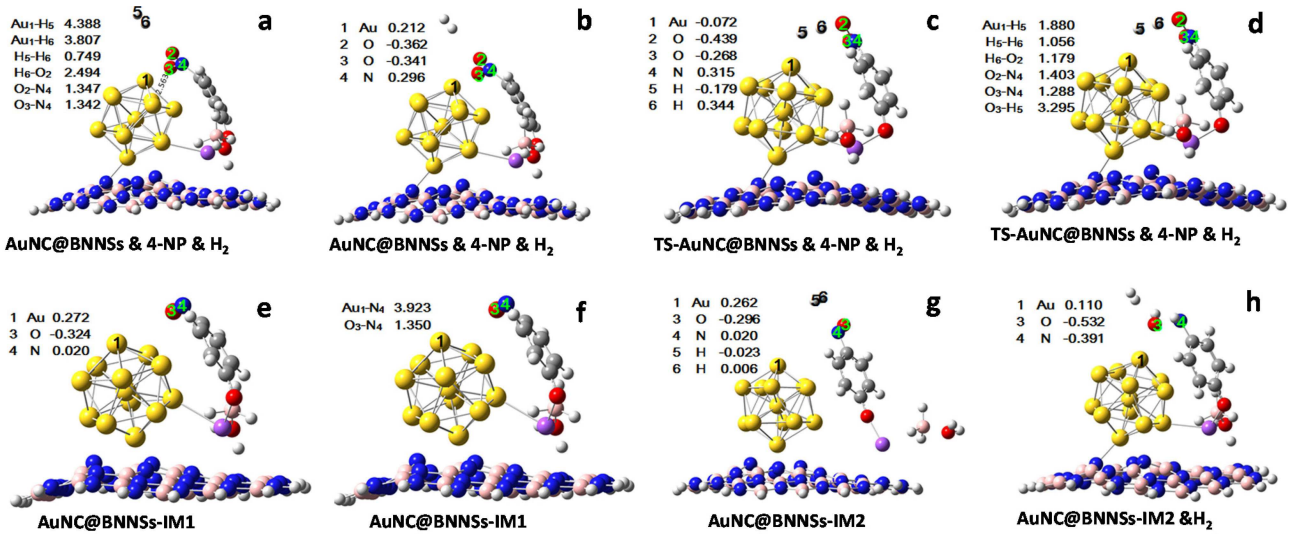


**Figure 5.** The charges and distances of selected atoms in the intermediates and transition states.

are−0.391 and−0.532 (Figure 5h), respectively. Therefore, the third molecule of hydrogen are attracted by N and O atoms, which is identified by the simulated result (Seen AuNC@BNNSs-IM2 & $H_2$). After the second water molecule is released, AuNC@BNNSs & 4-AP is formed (In Row 11 Figure S6). HOMO is well distributed in AuNCs and 4-AP so that the repulsion favors the release of 4-AP. By comparing Figure 4 and Figure 5, the following conclusion can be drawn. In the presence of BNNSs, electrons transfer from benzene ring in 4-NP to AuNCs which is the active center. Meanwhile, electron density on oxygen (O–H) in 4-NP is decreased which is helpful for deprotonation of 4-NP, and BNNSs keep 4-nitrophenolate ions at the vicinity of AuNCs, which is consistent with the previous report.[28] Secondly, electrons on HOMO repeatedly transfer between 4-NP and AuNCs supported on BNNS, which will make contribution to the enhanced catalytic activity of AuNC@BNNSs. Lastly, it has been proved that support-free catalyst showed serious aggregation and low catalytic activity.[29] Therefore, the catalytic performance could also be improved via the interaction between gold clusters and BNNSs, while preventing the aggregation of AuNCs.

## Conclusions

In summary, we have, using a facile, green and effective approach, synthesized AuNC@BNNSs nanohybrid, in which AuNCs with an average size of 1.5 nm are well distributed on BNNSs. Compared with the pure AuNC, the as-prepared AuNC@BNNSs nanohybrid not only exhibits much better catalytic activity for reduction of 4-NP, but also prevents aggregation of AuNCs even after several catalytical recycles. From the theoretical calculation based on DFT theory, it is demonstrated that remarkable improvement of catalytic activity is due to repeated electron transfer of HOMO between 4-NP and BNNSs mediated by AuNCs.Furthermore, the theoretical calculations indicate that the actual reducing agent is molecular hydrogen rather than borohydride. We expected that the current study could provide valuable clues to open new avenues to explore the potential applications of BNNSs nanohybrids with metallic nanoparticles in catalysis and other applications.

## Experimental Section

### Materials

Boron nitride powder (1 μm in average diameter), 4-nitrophenol (AR, 99%), sodium borohydride ($NaBH_4$) (98%) and glutathione (GSH) were obtained from Aladdin (Shanghai, China). Tetrachloroauric acid ($HAuCl_4$) (AR) was purchased from Sigma-Aldrich (Shanghai, China). Sodium hydroxide (NaOH), potassium hydroxide (KOH) and hydrochloric acid (HCl) were purchased from Tianjin Guangfu technology development reagent (Tianjin, China). Ultrapure water (18.2 $M\Omega\,cm^{-1}$) was obtained from a Milli-Q ultrapure system (Qingdao, China). All of the chemicals were used as supplied without further purification.

### Preparation of BNNSs by Ball Milling

2 g of the pristine h-BN powder, 20 mL aqueous NaOH solution (2 M) and 20 mL aqueous KOH solution (2 M) were loaded into a steel grinding bowl with 3 mm steel balls in diameter at ball-to-powder ratio of 50:1. The rotational speed of the planetary mill was set at 300 rpm to generate rolling actions of the balls, which exert shearing forces on h-BN powder, and the mixture was milled for 24 hours. The milled product was collected and rinsed with HCl solution (2 M) to remove the remaining residual like $Fe_2O_3$ and the alkaline solution and then repeatedly washed with deionized (DI) water until the pH was close to neutral. The samples were dried in a vacuum oven and re-dispersed in DI water at an initial concentration of 1 mg/mL.

### Preparation of Au Nanoclusters (AuNCs) on BNNSs Support (AuNC@BNNSs)

2 mL of BNNSs aqueous dispersion (1 mg/mL) was mixed with a solution containing 7 mL deionized water and 50 mg glutathione, followed by the addition of 1 mL $HAuCl_4$ aqueous solution (2 wt%) and then sonicated for 10 min in an ice-water bath. The resulting mixture was continually sonicated for 20 min and then transferred to a glass bottle and treated at 90 °C for 12 h to afford the AuNC@BNNSs nanohybrid, which was collected by centrifugation and repeatedly washed with DI water for three times. Finally, the aqueous suspension of AuNC@BNNSs was obtained and stored at 4 °C for subsequent usage.

### Catalytic Activity Investigation

The catalytic activity of the as-prepared AuNC@BNNSs nanohybrid was investigated by the reduction of 4-nitrophenol (4-NP). In a typical experiment, 1 mL of fresh $NaBH_4$ aqueous solution (0.02 M) and 2 mL of 4-NP aqueous solution (0.2 mM) were added into a quartz cuvette, following by the addition of 25 μL of AuNC@BNNSs aqueous suspension. The UV-vis absorption spectra were recorded to monitor the catalytic reaction in the wavelength range of 200–550 nm. The bright yellow color of the reaction mixture faded gradually to colorless during the catalytic reaction. In order to evaluate the effect of pH values on the catalytic activity, the pH value of the reaction mixture was adjusted with HCl solution. The recyclability of AuNC@BNNSs nanohybrid was tested by separating the catalyst from the reaction mixture via centrifugation at 15000 rpm for 15 min and immediately reused it for the same catalytic reaction under the same conditions.

## *Acknowledgements*

This work was supported by National Science Foundation of China (21675075) and Qingdao Innovation Leading Expert Program. We would also like to thank Australian Research Council (DP130101714) for financial support.

## *Conflict of Interest*

The authors declare no conflict of interest.

**Keywords:** boron nitride nanosheet · catalytic reduction · gold nanocluster · DFT theory · 4-nitrophenol

[1] a) Z. Zhang, C. Liu, R. E. Kinder, X. Han, H. Qian, R. A. Widenhoefer, *J. Am. Chem. Soc.* **2006**, *128*, 9066–9073; b) A. S. K. Hashmi, *Cheminform* **2007**, *38*, 3180–3211; c) M. Sankar, N. Dimitratos, P. J. Miedziak, P. P. Wells, C. J. Kiely, G. J. Hutchings, *Chem. Soc. Rev.* **2013**, *44*, 8099–8139; d) P. Luo, C. Li, G. Shi, *Phys. Chem. Chem. Phys.* **2012**, *14*, 7360–6; e) B. E. Hayden, D. Pletcher, J. P. Suchsland, *Angew. Chem. Int. Edit.* **2007**, *46*, 3530–3532; f) B. E. Hayden, D. Pletcher, J. P. Suchsland, *Angew. Chem. Int. Edit.* **2010**, *46*, 3530–3532.
[2] H. Qian, M. Zhu, Z. Wu, R. Jin, *Acc. Chem. Res.* **2012**, *45*, 1470–1479.
[3] a) Caixia Xu, Jixin Su, Xiaohong Xu, Pengpeng Liu, Hongjuan Zhao, F. Tian, Y. Ding, *J. Am. Chem. Soc.* **2007**, *129*, 42–43; b) H. Tsunoyama, H. Sakurai, Y. Negishi, T. Tsukuda, *J. Am. Chem. Soc.* **2005**, *127*, 9374–9375; c) M. Turner, V. B. Golovko, O. P. Vaughan, P. Abdulkin, A. Berenguer-Murcia, M. S. Tikhov, B. F. Johnson, R. M. Lambert, *Nature* **2008**, *454*, 981–983.
[4] a) C. Huang, X. Ye, C. Chen, S. Lin, D. Xie, *Comput. Theor. Chem.* **2013**, *1011*, 5–10; b) B. L. Hendriksen, J. W. Frenken, *Phys. Rev. Lett.* **2002**, *89*, 046101–4; c) H. Y. Su, M. M. Yang, X. H. Bao, W. X. Li, *J. Phys. Chem. C* **2008**, *112*, 17303–17310; d) M. Zhao, L. Sun, R. M. Crooks, *J. Am. Chem. Soc.* **1998**, *120*, 4877–4878.
[5] a) J. Schornbaum, B. Winter, S. P. Schießl, F. Gannott, G. Katsukis, D. M. Guldi, E. Spiecker, J. Zaumseil, *Adv. Funct. Mater.* **2015**, *24*, 5798–5806; b) E. K. Jeon, E. Seo, E. Lee, W. Lee, M. K. Um, B. S. Kim, *Chem. Commun.* **2013**, *49*, 3392–3394.
[6] X. Ke, S. Sarina, J. Zhao, X. Zhang, J. Chang, H. Zhu, *Chem. Commun.* **2012**, *48*, 3509–3511.
[7] J. J. Spivey, *Ind. Eng. Chem. Res.* **1989**, *26*, 2165–2180.
[8] Z. Yan, S. Chinta, A. A. Mohamed, J. P. Fackler, D. W. Goodman, *J. Am. Chem. Soc.* **2005**, *127*, 1604–5.
[9] a) S. Lee, C. Fan, T. Wu, S. L. Anderson, *J. Am. Chem. Soc.* **2004**, *126*, 5682–5683; b) H. Zhu, N. Goswami, Q. Yao, T. Chen, Y. Liu, Q. Xu, D. Chen, J. M. Lu, J. Xie, *J. Mater. Chem. A* **2018**, *6*. 1102–1108
[10] P. Kundu, C. Nethravathi, P. A. Deshpande, M. Rajamathi, G. Madras, N. Ravishankar, *Chem. Mater.* **2011**, *23*, 2772–2780.
[11] a) Z. Song, W. Li, F. Niu, Y. Xu, L. Niu, W. Yang, Y. Wang, J. Liu, *J. Mater. Chem. A* **2017**, *5*, 230–239; b) H. Yan, H. Cheng, H. Yi, Y. Lin, T. Yao, C. Wang, J. Li, S. Wei, J. Lu, *J. Am. Chem. Soc.* **2015**, *137*, 10484–10487; c) C. Wang, H. Wang, C. Zhai, F. Ren, M. Zhu, P. Yang, Y. Du, *J. Mater. Chem. A* **2015**, *3*, 4389–4398.
[12] S. Shao, Z. Chi, L. Yuwen, C. Jie, X. Zuo, X. Liu, C. Song, C. Fan, L. Wang, *Acs Appl. Mater. Interfaces* **2014**, *6*, 18735–18741.
[13] a) L. Chen, X. Zeng, P. Si, Y. Chen, Y. Chi, D. H. Kim, G. Chen, *Anal. Chem.* **2014**, *86*, 4188–4195; b) G. Vilé, D. Albani, M. Nachtegaal, Z. Chen, D. Dontsova, M. Antonietti, N. López, J. Pérezramírez, *Angew. Chem. Int. Edit.* **2015**, *54*, 11265–11269.
[14] L. Wang, S. Q. Ni, C. Guo, Y. Qian, *J. Mater. Chem. A* **2013**, *1*, 6379–6387.
[15] a) C. A. Lin, J. C. S. Wu, J. W. Pan, C. T. Yeh, *J. Catal.* **2002**, *210*, 39–45; b) J. C. S. Wu, A. Yachun Fan, C. A. Lin, *Ind. Eng. Chem. Res.* **2003**, *42*, 3225–3229; c) W. Sun, Y. Meng, Q. Fu, F. Wang, G. Wang, W. Gao, X. C. Huang, F. Lu, *Acs Appl. Mater. Interfaces* **2016**, *8*, 9881–9888.
[16] N. Meyer, M. Devillers, S. Hermans, *Catal. Today* **2015**, *241*, 200–207.
[17] a) J. Xu, H. Shen, C. Duan, J. Guo, N. Zhao, *J. Mater. Chem. A* **2015**, *3*, 16663–16669; b) Y. Lin, C. E. Bunker, K. A. S. Fernando, J. W. Connell, *Acs Appl Mater Interfaces* **2012**, *4*, 1110; c) F. Wang, X. Zeng, Y. Yao, R. Sun, J. Xu, C. P. Wong, *Sci. Rep.* **2016**, *6*, 19394; d) X. Qiu, Q. Liu, M. Song, C. Huang, *J. Colloid. Interf. Sci.* **2016**, *477*, 131–137.
[18] a) M. Gao, A. Lyalin, T. Taketsugu, *J. Chem. Phys.* **2013**, *138*, 034701; b) A. K. Roy, S. Y. Park, I. In, *Nanotechnology* **2015**, *26*, 105601–8; c) L. Fu, G. Chen, N. Jiang, J. Yu, C. T. Lin, A. Yu, *J. Mater. Chem. A* **2016**, *4*, 19107–19115; d) Q. Liu, Y. Xu, X. Qiu, C. Huang, M. Liu, *J. Catal.* **2019**, *370*, 55–60.
[19] L. Fu, G. Chen, N. Jiang, J. Yu, C.-T. Lin, A. Yu, *J. Mater. Chem. A* **2016**, *4*, 19107–19115.
[20] a) G. Lai, J. Wu, H. Ju, F. Yan, *Advanced Functional Materials* **2011**, *21*, 2938–2943; b) Q. Lu, J. Deng, Y. Hou, H. Wang, H. Li, Y. Zhang, S. Yao, *Chem. Commun.* **2015**, *51*, 7164–7167; c) P. Raveendran, J. Fu, S. L. Wallen, *J. Am. Chem. Soc.* **2003**, *125*, 13940–13941; d) I. Washio, Y. Xiong, Y. Yin, Y. Xia, *Adv. Mater.* **2006**, *18*, 1745–1749.
[21] L. Shang, R. M. Dörlich, S. Brandholt, R. Schneider, V. Trouillet, M. Bruns, D. Gerthsen, G. U. Nienhaus, *Nanoscale* **2011**, *3*, 2009–2014.
[22] J. Ftouni, M. Penhoat, A. Addad, E. Payen, C. Rolando, J.-S. Girardon, *Nanoscale* **2012**, *4*, 4450–4454.
[23] a) L. Lin, Y. Xu, S. Zhang, I. M. Ross, A. C. Ong, D. A. Allwood, *Small* **2014**, *10*, 60–65; b) D. Lee, B. Lee, K. H. Park, H. J. Ryu, S. Jeon, S. H. Hong, *Nano Letters* **2015**, *15*, 1238–1244; c) B. Liu, S. Yan, Z. Song, M. Liu, X. Ji, W. Yang, J. Liu, *Chemistry* **2016**, *22*, 18899–18907.
[24] H. S. Lim, W. O. Jin, S. Y. Kim, M. J. Yoo, S. D. Park, W. S. Lee, *Chem. Mater.* **2013**, *25*, 3315–3319.
[25] W. Teng, B. Jin, Z. Jiao, G. Lu, J. Ye, Y. Bi, *J. Mater. Chem. A* **2014**, *2*, 12–20.
[26] a) S. Saha, A. Pal, S. Kundu, S. Basu, T. Pal, *Langmuir* **2010**, *26*, 2885–2893; b) G. Rothenberg, *Concets, green application*, Wiley-VCH Verlag Gmbh & Co. KGaA: Weinheim, **2008**, p 11.
[27] a) H. I. Schlesinger, H. C. Brown, A. E. Finholt, J. R. Gilbreath, H. R. Hoekstra, E. K. Hyde, *J. Am. Chem. Soc.* **1953**, *75*, 215–219; b) W. Xie, R. Grzeschik, S. Schlücker, *Angew. Chem Int. Edit.* **2016**, *128*, 13933–13937; c) S. C. Amendola, S. L. Sharp-Goldman, M. S. Janjua, M. T. Kelly, P. J. Petillo, M. Binder, *J. Power Sources* **2000**, *85*, 186–189.
[28] a) C. Huang, W. Ye, Q. Liu, X. Qiu, *ACS Appl. Mater. Interfaces* **2014**, *6*, 14469–14476. b) Q. Liu, C. Chen, M. Du, Y. Wu, C. Ren, K. Ding, M. Song, C Huang, *ACS Appl.Nano.Mater.* **2018**, *1*, 4566–4575.
[29] X. Yang, J. Sun, M. Kitta, H. Pang, Q. Xu, *Nat. Catal.* **2018**, *1*, 214–220.

Manuscript received: March 3, 2019
Version of record online: April 4, 2019